ADVANCED MATERIALS INTERFACES
Open Access
www.advmatinterfaces.de

Capillary Adhesion around the Shapes Optimized by Dissolution

*Xudong Chen and Quanzi Yuan**

Capillary adhesion is so remarkable in micro–nano technology that it can seriously influence accuracy and safety. The shapes optimized by dissolution provide a method to weaken or even eliminate capillary adhesion. Based on the dissolution experiments of soluble fibers, this work demonstrates that the process of dissolution is an optimization of the adhesion force, and the unique geometrical shapes sculpted by dissolution can effectively eliminate capillary adhesion. The mechanism of elimination is relevant to the stability of menisci around the optimized shapes. The surface roughness of soluble fibers is considered to emphasize the significant role of contact angle hysteresis (CAH), and the shapes optimized by dissolution with CAH are in great agreement with the experiment results. This study supplies a promising approach to eliminate capillary adhesion by designing geometrical shapes.

1. Introduction

The liquid menisci between two lyophilic substrates cause attractive forces, namely capillary adhesion.[1] It is well-known that wetting sand is necessary to build a sand castle because wet sand can be shaped while dry sand flows easily.[2] The alternation of capillary adhesion is generally achieved by chemical technology or physical modification.[3] For chemical technology, coatings[4] and self-assembly structures[5] are used to change the surface wettability. For physical modification, geometrical structures and surface roughness are important factors affecting capillary adhesion.[6] In particular, the geometrical design of structures as an effective method still needs to be improved. Moreover, liquids or droplets are usually pinned on the substrate surfaces, which strongly influences the formation of capillary adhesion. This phenomenon can be described by contact angle hysteresis (CAH), which is a difference between advancing and receding angles.[7] The main causes invoked for the CAH are surface roughness, external fields, and heterogeneities. We focused on these factors in this work. Furthermore, the adhesion force is crucial to micro–nano technology.[8–11] For example, the accuracy and safety of measurements performed with the atomic force microscope (AFM) are strongly influenced by capillary adhesion[12] due to spontaneous capillary condensation in a humid environment. Although fluorosilane coating can be used for AFM tips to increase hydrophobicity, the challenges posed by chemical treatment are still very difficult to overcome.[13] The topography of substrates provides an effective method to weaken capillary adhesion, such as the walls of pollen cells.[14] The spiky particles with nanometric asperities are robust to desiccation and rehydration.[15] However, the mechanism behind the weakening of capillary adhesion by the spiky configuration is poorly studied, which hitherto remains an open question.

In this work, we designed the geometrical shapes of tips to weaken or even eliminate capillary adhesion based on dissolution experiments and explored the physical mechanism underlying unique geometry. Based on the systematic and elegant works of previous researchers on the electrochemical etching of tips for scanning tunneling microscopy,[16–19] we developed dissolution experiments where tungsten filaments dissolve into an aqueous potassium hydroxide solution under external electric fields. We will demonstrate that the contact line slips off the surfaces of vertical soluble cylinders submerged partially in an infinite solution bath, transforming the cylinders into unique geometrical shapes with low capillary adhesion. In other words, this process of dissolution is an optimization of capillary adhesion. Moreover, the CAH is introduced to consider surface roughness, external fields, and heterogeneities. The shapes sculpted by dissolution with CAH are consistent with the experiment results, which can provide an instructive calculation model for experiments.

2. Results and Discussion

As is well-known, a liquid meniscus forms around a lyophilic circular cylinder immersed partially in an infinite liquid bath

X. Chen, Q. Yuan
State Key Laboratory of Nonlinear Mechanics
Institute of Mechanics
Chinese Academy of Sciences
Beijing 100190, P. R. China
E-mail: yuanquanzi@lnm.imech.ac.cn
X. Chen, Q. Yuan
School of Engineering Science
University of Chinese Academy of Sciences
Beijing 100049, P. R. China

The ORCID identification number(s) for the author(s) of this article can be found under https://doi.org/10.1002/admi.202202380.

DOI: 10.1002/admi.202202380

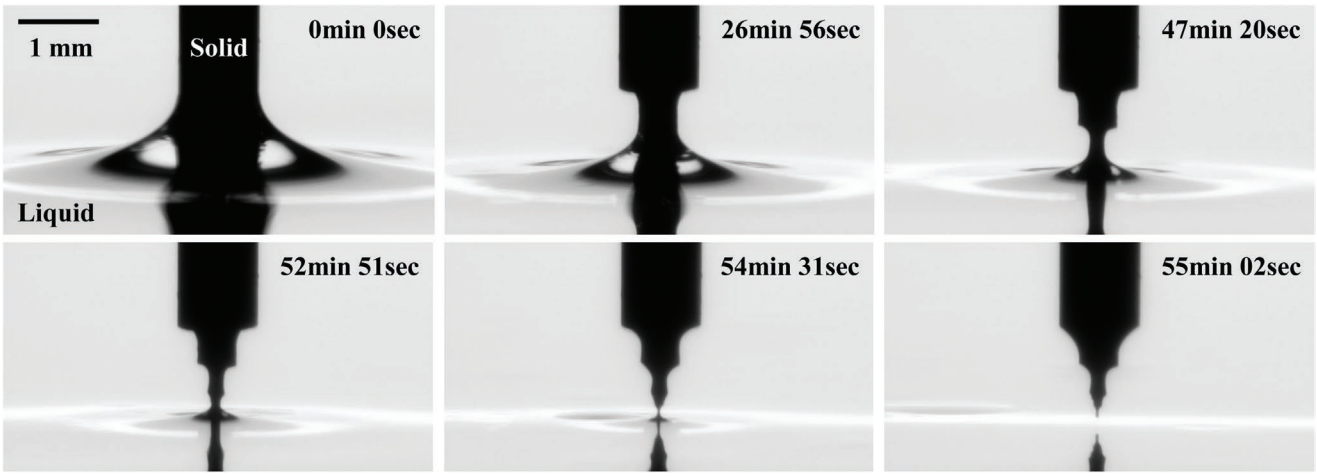

Figure 1. Images captured by the camera in the dissolution experiment at different moments.

in a downward gravity field, leading to capillary adhesion. In terms of soluble fibers dipped vertically into a solution, menisci gradually slide down along the walls of soluble fibers as the solute dissolves in the solvent, which converts the cylindrical configuration into the shapes like tips, as shown in **Figure 1**.

2.1. Analyses of Interfaces in Dissolution

Figure 2 shows the schematic diagrams of dissolution experiments. A vertical soluble cylindrical filament with a radius of r_0 is partially submerged in a liquid bath extending to infinity. The meniscus around the filament is determined by its radius r_0 and contact angle α, as illustrated in Figure 2a. Therefore, the governing equations of the meniscus can be written as[20]

$$\frac{\mathrm{d}R}{\mathrm{d}\psi}=\frac{R\cos\psi}{\kappa RU-\sin\psi},\quad \frac{\mathrm{d}U}{\mathrm{d}\psi}=\frac{R\sin\psi}{\kappa RU-\sin\psi} \tag{1}$$

with the boundary conditions

$$R=1\,\text{at}\,\psi=\pi/2-\alpha \tag{2}$$

$$U\to 0\,\text{and}\,R\to\infty\,\text{as}\,\psi\to 0 \tag{3}$$

where $\kappa=\rho g/\gamma$ is the capillary constant with the density of the solution ρ, gravitational acceleration g, and the interface energy per unit area of liquid–vapor interfaces γ. The inclination angle of the meniscus is denoted by ψ. In addition, we introduce the dimensionless coordinate system (R, U), with respect to the radius r_0. In this process of dissolution, the soluble cylinder spontaneously dissolves into the liquid, resulting in the alternation of its geometrical shape. Furthermore, as the evolution of its shape changes the boundary conditions of the meniscus, the contact line slides down along the sculpted surface. The meniscus around the soluble cylinder will achieve stability under new boundary conditions, as seen in Figure 2b. After that, the decline of the meniscus continues to occur periodically until the solute separates from the liquid bath, as shown in Figure 2c. It is remarkable that the cylindrical configuration of the filament is converted into a unique wave-like shape, similar to the results of experiments in Figure 2d.

To investigate the formation of the unique wave-like shape sculpted by dissolution, we proposed models of dissolution for the vertical soluble cylinders immersed partially in an infinity liquid bath. It is worth noting that the receding of the contact line is slow enough to be regarded as a quasi-static process. In this process, the alteration of soluble cylinder surfaces induced

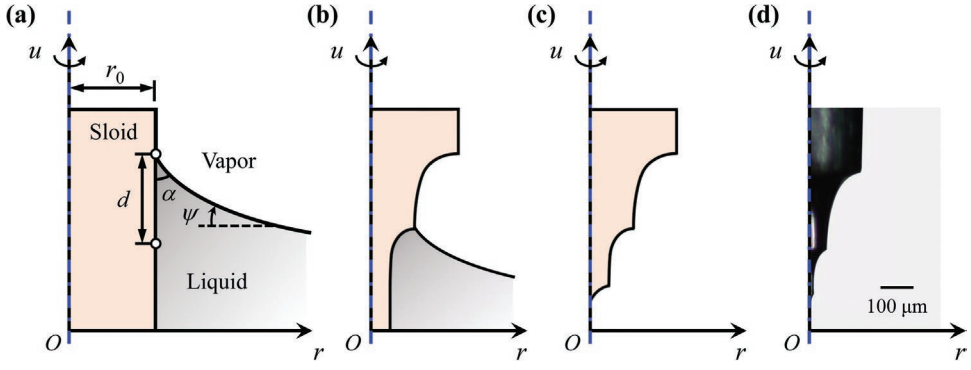

Figure 2. a–c) Schematics of dissolution where soluble cylindrical filaments are partially immersed in an infinity liquid bath, representing initial state, transitional state, and final state, respectively. d) An optical image of experimental results.

ADVANCED MATERIALS INTERFACES
Open Access
www.advmatinterfaces.de

by shear stresses can be ignored because the flow velocity of the liquid is quite slow. Therefore, we assumed that the Péclet number (Pe = V_0L/D, V_0 is the characteristic velocity of convection, L is the characteristic length, and D is the diffusion coefficient)[21] that describes the transportation of the solute dissolved in the solvent is much less than one. It indicates that diffusion dominates the transport of solute in solution rather than convection. In general, diffusion is the spontaneous transport of solute from the regions of higher concentration to the ones of lower concentration based on the Fick law.[22] According to the profile of the axisymmetric meniscus around a cylinder mentioned above, it is concluded that the concentration of solute at the contact line tends to be saturated, corresponding to the minimal velocity of dissolution $V_{\min}$. Moreover, the maximum velocity of dissolution $V_{\max}$ is adjacent to the reference level $u = 0$ due to the liquid extending to infinity. As stated by the above analyses, the shape evolution of soluble cylinders, a function of time, can be represented by the diffusion velocity of solute at the solid–liquid interface, which is concisely assumed as linear at first.

$$V = \begin{cases} V_{\max}, & \text{for } d > \eta r \\ V_{\min} + (V_{\max} - V_{\min})\left[d/(\eta r)\right], & \text{for } d \le \eta r \end{cases} \tag{4}$$

where d is the vertical distance from the contact line in Figure 2a, r is the local radius at the contact line, and η is an experiential coefficient. The maximum velocity of dissolution $V_{\max}$ and the experiential coefficient η depends on the solubility of soluble cylinders and the solution environment. In addition to the linear hypothesis, a few solutes transport from the regions of higher chemical potential to the ones of lower chemical potential, which is described by the Cahn–Hilliard equation.[23] For this reason, the velocity of dissolution V is necessary to be represented by the Boltzmann distribution.[24]

$$V = V_{\max} + 2(V_{\min} - V_{\max}) / \left\{1 + \exp\left[d/(\eta r)\right]\right\} \tag{5}$$

With the variation of boundary conditions governed by the velocities of dissolution, the menisci around soluble cylinders with r_0 = 100 µm are calculated numerically, as shown in **Figure 3**. The following parameters of an aqueous potassium hydroxide solution with the concentration 2 mol L^{-1} are used: ρ = 1090 kg m^{-3}, g = 9.8 m s^{-2}, γ = 0.042 N m^{-1}, $\alpha = 0$. Given that the concentration of solution at the contact line is saturated in the process of dissolution, $V_{\min} = 0$ and $V_{\max} = r_0/100$. In Figure 3, the solid–liquid interface and the liquid–vapor interface with the same color are simultaneous. The evolution of time is indicated by the color from light to dark. The results show that the height of the meniscus continuously decreases, and eventually drops to zero, coinciding with the reference level $U = 0$. It is noteworthy that the shapes sculpted by the process of dissolution are almost identical whether at the linear dissolution velocity or the Boltzmann one. Both of them can be characterized as dimensionless expression $U = aR^m$, which is fairly consistent with the sculpted geometrical shapes, with the same coefficient a and exponent m. The coefficient a is the initial dimensionless height of the meniscus. Moreover, the capillary adhesion around the cylinders decreases continuously as the shapes develop, and disappears finally when the soluble

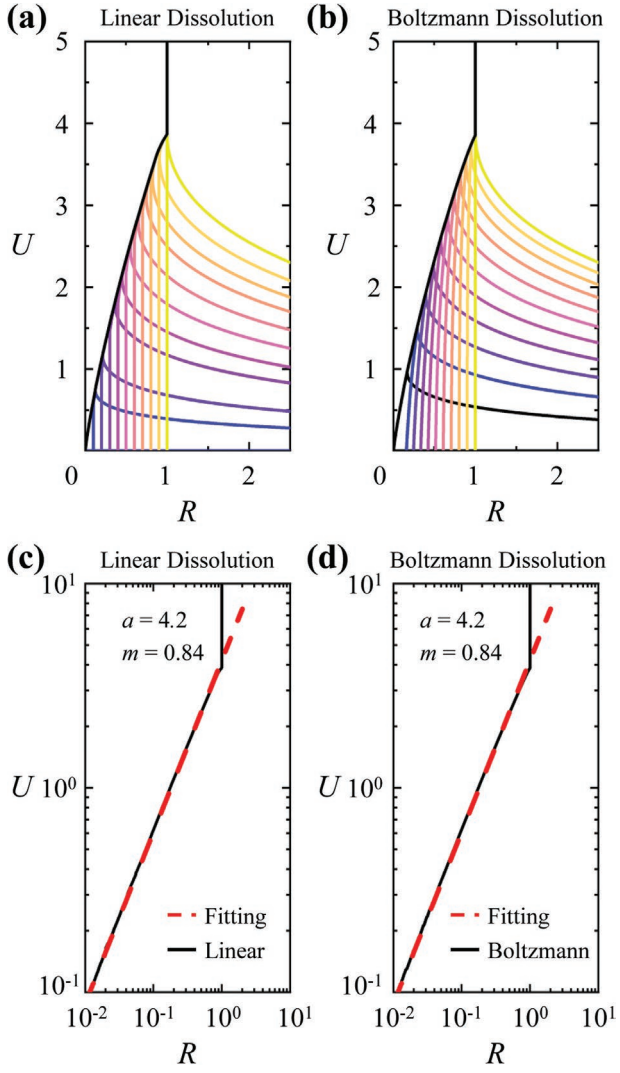

Figure 3. The geometrical shapes of soluble cylinders optimized by dissolution. The quasi-static process of cylinders with 100 µm at a) linear velocity and b) Boltzmann velocity. The colors of solid–liquid interfaces (intersecting with the line $U = 0$) are the same as the colors of liquid–vapor interfaces (intersecting with the line $R = 2.5$) at the same moment, and the development of time is indicated by the color from light to dark. The final shapes optimized by dissolution at c) linear velocity and d) Boltzmann velocity, denoted by black solid lines. The red dashed lines denote the fitting curves represented by the power function $U = aR^m$.

cylinders separate from the liquid. This decrease in capillary adhesion indicates that the process where vertical soluble cylinders dissolve in an infinity liquid bath is an optimization one.

2.2. Discussion on the Shapes Optimized by Dissolution

As stated by the discussion of the geometrical shapes during the process of dissolution, the optimized shapes characterized as $U = aR^m$ own the property of eliminating capillary adhesion. The coefficient a represents the initial conditions. The exponent m determines the geometry of the optimized shapes to prevent the formation of menisci. Therefore, we

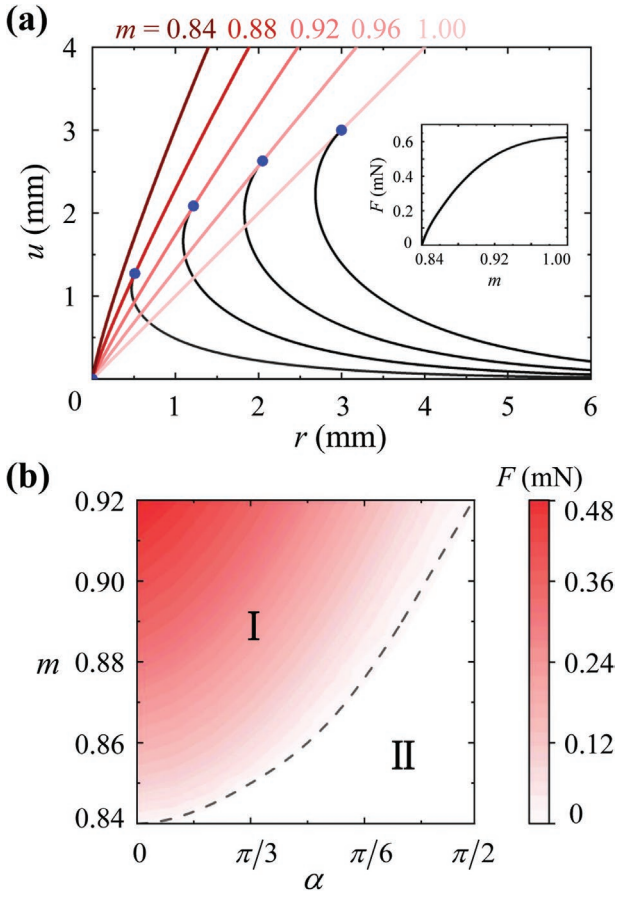

Figure 4. The capillary adhesion force around the unique shapes characterized by $u = r^m$. a) The height of menisci on the surfaces represented by different exponents m. The red lines denote the profiles of the unique shapes and the black lines denote the liquid–vapor interfaces. Inset: the relationship between the capillary adhesion force F and the exponent m. b) The contour lines of the adhesion force F at different contact angles α around the shapes represented by different exponents m. The black dashed line denotes the relationship curve between the critical exponent m^* and the contact angle α, dividing this map into region I (menisci can form) and region Π (not).

adopted $u = r^m$ as the geometrical shapes of cones to investigate the restriction of the shapes optimized by dissolution on the capillary adhesion. The horizontal component of capillary adhesion is in equilibrium for these axisymmetric configurations, and the vertical one F is composed of the pressure force F_P and surface tension F_T. It has been proven that the vertical component of adhesion F is equal to the weight of the liquid which fills the region bounded below by the meniscus and the wetted surface, and above by the reference level $U = 0$.[25]

According to the above analyses, the results of the menisci and capillary adhesion around the particular cones are reported in **Figure 4**. The menisci decline as the exponent m changes from light red to dark red. Compared to the initial case ($m = 1$), both the height of menisci and capillary adhesion around cones slide down when m decreases, as shown in Figure 4a. Finally, we can observe that there is a critical exponent $m^* = 0.84$, satisfying that the meniscus fails to form around the cones characterized by $u = r^m$ ($m < m^*$). In other words, these cones in unique shapes own the property of eliminating capillary adhesion. The underlying reason for this fact is that the menisci around the cones with exponent $m < m^*$ are unstable, each of which exceeds the critical state.[26] Essentially, the second variation of the total potential energy of this system is negative for certain disturbances of the liquid–vapor interface,[27] causing the instability of menisci (details in the Supporting Information). Furthermore, we also calculated capillary adhesion forces around the unique cones at different contact angles for the aqueous potassium hydroxide solution. As shown in Figure 4b, the results imply that the adhesion force F will decline at all contact angles when m decreases. The relationship curve between the critical exponent m^* and the contact angle α divides the results into two cases (menisci can form or not) in Figure 4b.

2.3. Dissolution with Contact Angle Hysteresis

Comparing the optimized cones characterized by power functions with the experimental results, the wave-like shapes obtained from experiments remain clouded. Interestingly, the CAH provides us with a promising method to explore this phenomenon. According to the above considerations, due to the change of boundary conditions governed by the velocities of dissolution, the menisci around soluble cylinders decline gradually until the solute separates from the solution bath. The contact angle α in boundary conditions is determined by the Young–Laplace equation for a pure liquid lying on a perfectly flat, rigid, and smooth substrate without any impurity or heterogeneity.[8] For real systems, however, the CAH will be measured with the advancing contact angle θ_a and the receding angle θ_r, because the contact line is pinned on the substrate. Therefore, the CAH as a significant factor needs to be considered in the process of dissolution, especially for the boundary conditions. We recalculated the shape evolution of vertical soluble cylinders submerged partially in an infinity solution bath under the boundary conditions controlled by CAH. The results are reported in **Figure 5**. At the beginning of dissolution, the meniscus forms around the soluble cylinder at the contact angle α, which is equal to the equilibrium contact angle θ_e. Given that θ_e is less than the advancing contact angle θ_a, the height of the contact line remains unchanged. While the soluble cylinder dissolves into the solution, the contact line is pinned at a fixed height due to the CAH, leading to a continuous increase in the contact angle α. The meniscus will be unstable when α increases to the advancing contact angle θ_a. At that moment, the liquid–vapor interface will decline until achieving new stability on the surface sculpted by dissolution, meanwhile satisfying $\alpha = \theta_e$. This process will develop periodically until the soluble cylinder separates from the liquid bath, and finally, the meniscus will coincide with the reference level $U = 0$. Similar to the cases without the CAH, the colors of liquid–vapor interfaces are the same as the ones of solid–liquid interfaces at the same moment. The evolution of time is indicated by the color from light to dark. Furthermore, based on Equations (4) and (5), we calculated the dissolution process of soluble cylinders with $r_0 = 100$ μm at the linear velocity and the Boltzmann one.

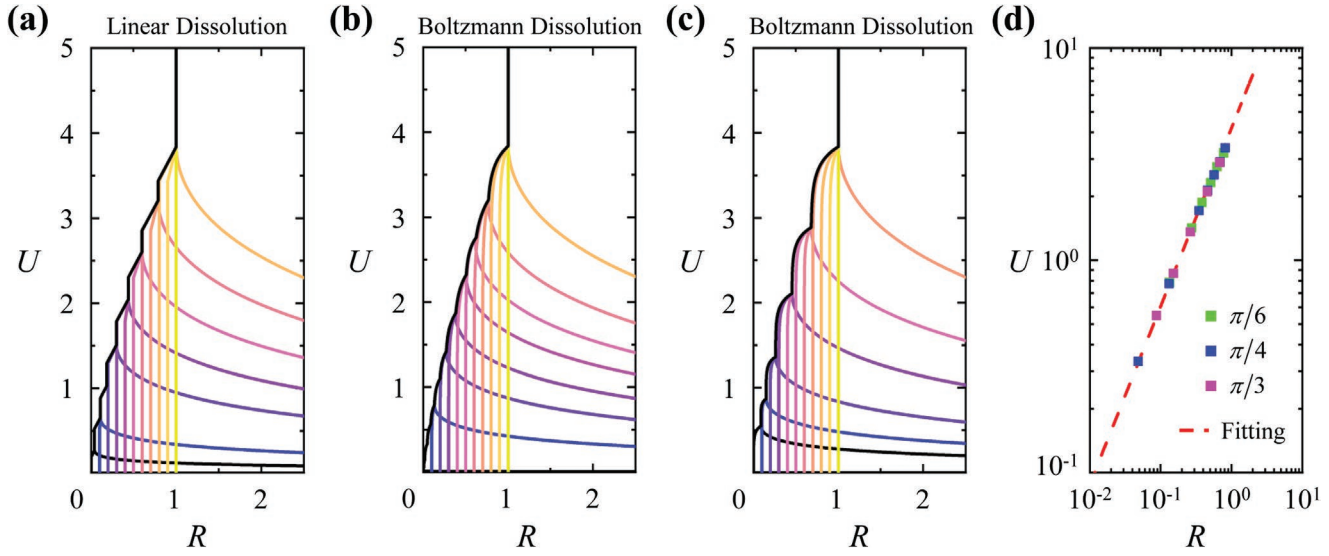

Figure 5. The analyses of geometrical shapes optimized by dissolution with contact angle hysteresis. a) The linear dissolution at the advancing angle $\theta_a = 30°$. The Boltzmann dissolution at b) $\theta_a = 30°$ and c) $\theta_a = 60°$. d) The sharp positions (square points) where the contact lines are pinned at different advancing angles, compared with the fitting curve $U = 4.2{*}R^{0.84}$ (the red dashed line).

Figure 5 shows that due to the influence of CAH on the process of dissolution, as reported by the above experimental results, the soluble cylinders are converted into unique wave-like shapes. However, the results at the linear velocity in Figure 5a present a zig-zag shape incompatible with the experimental results. This inconformity demonstrates that the hypothesis of linear dissolution does not apply to real systems with CAH. On the contrary, the results of the Boltzmann dissolution in Figures 5b and 4c describe the authentic process. When the contact lines are pinned on the surface, which corresponds to the overlap of menisci in different colors, the soluble cylinders keep dissolving at the Boltzmann velocity, causing the wave-like shapes. As the dissolution develops periodically, the sculpted waves become smaller and smaller until the solute separates from the liquid. For the case with increased CAH in Figure 5c, the characteristics in the process of dissolution are more apparent. We noticed that the amplitude of waves is larger than before, and the number of ones is smaller. Moreover, the bottom of the shapes optimized by dissolution overtops the reference level $U = 0$ due to the CAH. To explore the restriction of the wave-like shapes to capillary adhesion further, we compared the sharp positions where the contact lines are pinned with the shapes represented by $U = aR^m$ in Figure 5d. Surprisingly, all of the sharp positions coincide with the fitting curve. This result indicates that the wave-like shapes optimized by dissolution in real systems with CAH can eliminate capillary adhesion as well.[28]

2.4. Experimental Verification

To further validate the accuracy of the calculations, we performed dissolution experiments as follows: a vertical tungsten filament with a radius of 0.5 mm is partially submerged in an aqueous potassium hydroxide solution bath. An external electric field is applied to the above experimental system with the advancing angle 75°. The shape evolution of the tungsten filament is shown in **Figure 6**a.

The process of electrochemistry is the same as the calculation process of dissolution. The meniscus around the tungsten filament declines periodically until the filament separates from the solution. Eventually, the meniscus coincides with the reference level $U = 0$. Due to the unavoidable CAH, the bottom of the tungsten filament optimized by dissolution is above the reference level $U = 0$, and the waves of the optimized shape become smaller as the dissolution develops. Based on the experimental parameters, we calculated the shapes optimized by dissolution at the Boltzmann velocity, shown as the black line in Figure 6b. Comparing the calculation results with the experimental results in Figure 6b, it is concluded that the Boltzmann dissolution is in great agreement with the experiment process. This surprising degree of coincidence of calculations and experiments clearly indicates that we can design corresponding experiments to control geometrical shapes of soluble filaments, which own the property of eliminating capillary adhesion, based on the governing equations of menisci and the Boltzmann dissolution. For closely ideal systems, the simplified linear hypothesis can reflect the shapes optimized by dissolution as well. In addition, it is remarkable that external electric fields only provide a method to cause dissolution, and do not play a crucial role in such phenomena. Similar experiment results can be observed in non-electrochemical systems.[28]

3. Conclusion

In conclusion, our results clearly establish that the dissolution of vertical soluble cylinders partially immersed in an infinity liquid bath is an optimization of capillary adhesion, and the unique shapes optimized by dissolution can effectively eliminate capillary adhesion. Based on dissolution experiments, we presented the hypotheses of linear and Boltzmann velocities for

ADVANCED MATERIALS INTERFACES
Open Access
www.advmatinterfaces.de

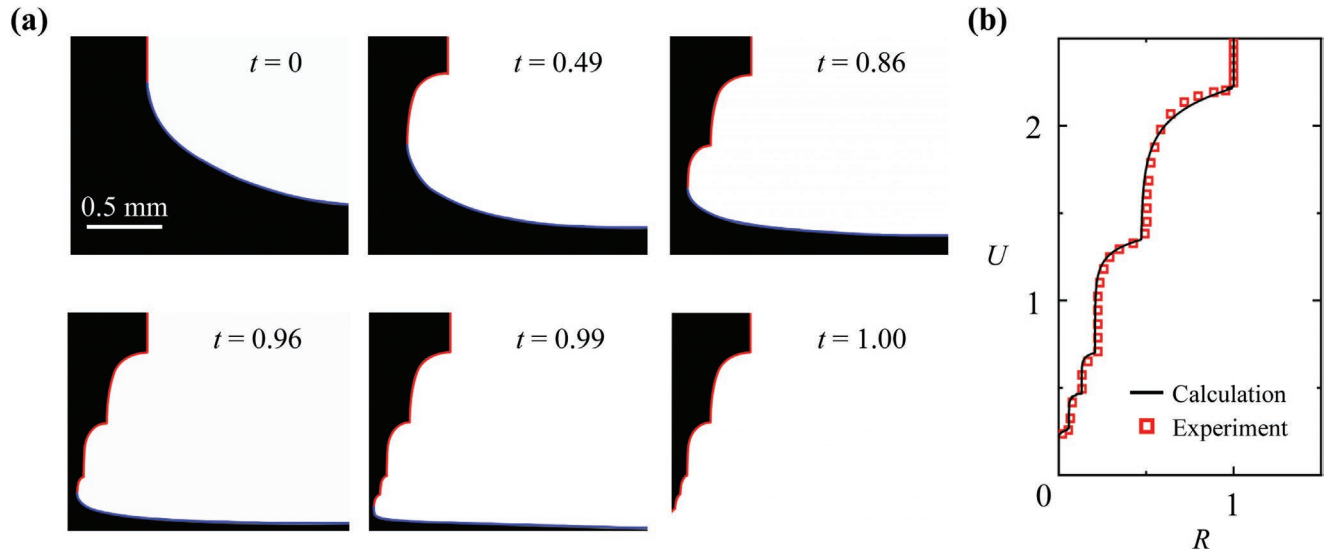

Figure 6. a) The dissolution process of a vertical tungsten filament with a radius of 0.5 mm submerged in an aqueous potassium hydroxide solution bath under an external electric field. The time recorded by the camera is normalized. The profiles of the tungsten filament and menisci are denoted by red and blue lines, respectively. b) Comparison between the calculation results and the experiment results.

the process of dissolution. For ideal systems with a pure liquid and a perfectly smooth substrate, the soluble cylindrical filaments are converted into the unique geometrical shapes characterized by $U = aR^m$ under both hypotheses. The exponent m plays a significant role in capillary adhesion. The critical exponent m^* satisfies that the meniscus fails to form around the cones represented by $u = r^m$ ($m < m^*$), eliminating capillary adhesion effectively. For real systems with surface roughness and heterogeneities, due to the CAH, the soluble cylinders are converted into the unique wave-like shapes similar to experiment results only under the hypothesis of Boltzmann dissolution. Moreover, the optimized wave-like shapes are directly relevant to the power function $U = aR^m$, which is concluded that the results of dissolution in real systems with CAH can eliminate capillary adhesion as well. Furthermore, electrochemical experiments are performed to verify the calculation results. The coincidence of both demonstrates that geometrical shapes of soluble filaments can be designed by corresponding experiments based on the mentioned calculation model. These promising results can enhance our knowledge of the pathways to overcome the disadvantages of capillary adhesion and reveal new insights into the application fields, such as optimized tips,[29] spiky particles,[30] and micro-needle arrays.[31,32]

4. Experimental Section

Sample Preparation: Due to the high mechanical strength and the highest melting point of tungsten, we developed specific dissolution experiments where tungsten filaments are submerged vertically in an aqueous potassium hydroxide solution with external electric fields applied to control dissolution. The tungsten filament as the positive pole is vertically submerged into the liquid bath. The bath as the negative pole is connected to a direct current (DC) power supply through a circular steel loop (schematic diagrams in the Supporting Information). The aqueous potassium hydroxide solution is prepared by analytically pure reagents and deionized water, which is placed in a 130 × 60 × 60 mm bath. The density of the solution is 1090 kg m^{-3} and the concentration is 2 mol L^{-1}. The surface tension is measured as 0.042 N m^{-1}. The tungsten filaments as soluble fibers with a purity of 99.99% are fixed on the lifting platform to reach the appropriate height. The external electric field is supplied by a constant voltage DC source. The voltage difference between the positive and negative poles is set as 9.0 V. The advancing angles are measured as 75° under this electric field. The ambient temperature is 22 °C. Images are captured by a camera from the side view.

Supporting Information

Supporting Information is available from the Wiley Online Library or from the author.

Acknowledgements

This work was jointly supported by the National Natural Science Foundation of China (NSFC, Grant No. 12072346), and the Open Fund of Key Laboratory for Intelligent Nano Materials and Devices of the Ministry of Education NJ2022002 (INMD-2022M01).

Conflict of Interest

The authors declare no conflict of interest.

Data Availability Statement

The data that support the findings of this study are available from the corresponding author upon reasonable request.

Keywords

capillary adhesion, contact angle hysteresis, dissolution, interfacial effects, liquid bridges

Received: November 18, 2022
Revised: January 31, 2023
Published online: April 4, 2023

[1] L. Bocquet, E. Charlaix, S. Ciliberto, J. Crassous, *Nature* **1998**, *396*, 735.
[2] T. C. Halsey, A. J. Levine, *Phys. Rev. Lett.* **1998**, *80*, 3141.
[3] H. Liu, J. Zhai, L. Jiang, *Soft Matter* **2006**, *2*, 811.
[4] S. H. Kim, D. B. Asay, M. T. Dugger, *Nano Today* **2007**, *2*, 22.
[5] S. Wang, L. Feng, H. Liu, T. Sun, X. Zhang, L. Jiang, D. Zhu, *ChemPhysChem* **2005**, *6*, 1475.
[6] H.-J. Butt, M. Kappl, *Adv. Colloid Interface Sci.* **2009**, *146*, 48.
[7] Q. Zeng, H. Zhou, J. Huang, Z. Guo, *Nanoscale* **2021**, *13*, 11734.
[8] B. Bhushan, Y. C. Jung, *Prog. Mater. Sci.* **2011**, *56*, 1.
[9] M. Srinivasarao, *Phys. Today* **2017**, *70*, 60.
[10] P. Saha, T. Duanis-Assaf, M. Reches, *Adv. Mater. Interfaces* **2020**, *7*, 2001115.
[11] Y. F. Dufrêne, D. Martínez-Martín, I. Medalsy, D. Alsteens, D. J. Müller, *Nat. Methods* **2013**, *10*, 847.
[12] R. Suriano, C. Credi, M. Levi, S. Turri, *Appl. Surf. Sci.* **2014**, *311*, 558.
[13] B. Bhushan, S. Martin, *J. Colloid Interface Sci.* **2018**, *526*, 90.
[14] E. Katifori, S. Alben, E. Cerda, D. R. Nelson, J. Dumais, *Proc. Natl. Acad. Sci. USA* **2010**, *107*, 7635.
[15] A. Radja, E. M. Horsley, M. O. Lavrentovich, A. M. Sweeney, *Cell* **2019**, *176*, 856.
[16] J. P. Ibe, P. P. Bey, S. L. Brandow, R. A. Brizzolara, N. A. Burnham, D. P. DiLella, K. P. Lee, C. R. K. Marrian, R. J. Colton, *J. Vac. Sci. Technol., A* **1990**, *8*, 3570.
[17] T. Hagedorn, M. E. Ouali, W. Paul, D. Oliver, Y. Miyahara, P. Grütter, *Rev. Sci. Instrum.* **2011**, *82*, 113903.
[18] B.-F. Ju, Y.-L. Chen, Y. Ge, *Rev. Sci. Instrum.* **2011**, *82*, 013707.
[19] W.-T. Chang, I.-S. Hwang, M.-T. Chang, C.-Y. Lin, W.-H. Hsu, J.-L. Hou, *Rev. Sci. Instrum.* **2012**, *83*, 083704.
[20] C. Huh, L. E. Scriven, *J. Colloid Interface Sci.* **1969**, *30*, 323.
[21] J. T. Padding, A. A. Louis, *Phys. Rev. E* **2006**, *74*, 031402.
[22] J. Weickert, in *Scale-Space Theory in Computer Vision*, Springer, Berlin **1997**, pp. 1–28.
[23] A. Novick-Cohen, in *Handbook of Differential Equations: Evolutionary Equations*, Elsevier, New York **2008**, pp. 201–228.
[24] A. J. M. Garrett, L. Poladian, *Ann. Phys.* **1988**, *188*, 386.
[25] J. B. Keller, *Phys. Fluids* **1998**, *10*, 3009.
[26] F. Zhang, X. Zhou, *J. Fluid Mech.* **2020**, *882*, A28.
[27] S. Ostrach, *Annu. Rev. Fluid Mech.* **1982**, *14*, 313.
[28] J. Yang, Q. Yuan, *Adv. Mater. Interfaces* **2022**, *9*, 2201248.
[29] A. Tuniz, M. A. Schmidt, *Nanophotonics* **2018**, *7*, 1279.
[30] S. Ito, S. N. Gorb, *ACS Appl. Mater. Interfaces* **2019**, *11*, 24691.
[31] W.-G. Bae, H. Ko, J.-Y. So, H. Yi, C.-H. Lee, D.-H. Lee, Y. Ahn, S.-H. Lee, K. Lee, J. Jun, H.-H. Kim, N. L. Jeon, W. Jung, C.-S. Song, T. Kim, Y.-C. Kim, H. E. Jeong, *Sci. Transl. Med.* **2019**, *11*, eaaw3329.
[32] J. Yu, Y. Zhang, Y. Ye, R. DiSanto, W. Sun, D. Ranson, F. S. Ligler, J. B. Buse, Z. Gu, *Proc. Natl. Acad. Sci. USA* **2015**, *112*, 8260.